11176-H304-R0-00

TRW NOTE NO. 69-FMT-765

PROJECT APOLLO
TASK MSC/TRW A-60.1

A PSEUDOSTATE THEORY FOR THE APPROXIMATION OF THREE-BODY TRAJECTORIES

Prepared for
MISSION PLANNING AND ANALYSIS DIVISION
NATIONAL AERONAUTICS AND SPACE ADMINISTRATION
MANNED SPACECRAFT CENTER
HOUSTON, TEXAS
NAS 9-8166

TRW SYSTEMS GROUP

CR 101862

11176-H304-R0-00

TRW NOTE NO. 69-FMT-765

PROJECT APOLLO
TASK MSC/TRW A-60.1

A PSEUDOSTATE THEORY FOR THE APPROXIMATION OF THREE-BODY TRAJECTORIES

Prepared for
MISSION PLANNING AND ANALYSIS DIVISION
NATIONAL AERONAUTICS AND SPACE ADMINISTRATION
MANNED SPACECRAFT CENTER
HOUSTON, TEXAS
NAS 9-8166

Prepared by S. W. Wilson, Jr.
S. W. Wilson, Jr.
Staff Engineer
Mission Simulation Department

Approved by P. G. Woodruff
P. G. Woodruff
Manager
Mission Simulation Department

Approved by
D. R. Davis
Manager
MSC/TRW Task A-60.1

Approved by R K Wright
D. P. Johnson
Assistant Project Manager
Mission Trajectory Control Program

TRW SYSTEMS GROUP

ABSTRACT

This document contains an analytical derivation and an empirical validation of a pseudostate theory for the approximation of three-body trajectories. Application of the theory yields "overlapped conic" trajectories characterized by error magnitudes only about 20 percent as great (for typical lunar missions) as patched conic trajectory errors. Execution time and adaptability to split boundary value problems are generally comparable, and in some cases the overlapped conic technique is superior to the patched conic method in both respects. Only minor changes in coding should be required to incorporate the overlapped conic simulation into existing patched conic computer programs. The overlapped conic simulation is currently being incorporated into the TRW Analytic Return-to-Earth Program - Moon Reference under MSC/TRW Task A-60.1. This document is submitted in partial fulfillment of the obligations of MSC/TRW Task A-60.1 for the Mission Trajectory Control Program, contract NAS9-8166.

CONTENTS

PRECEDING PAGE BLANK NOT FILMED.

ILLUSTRATIONS

NOMENCLATURE

Symbol	Definition
C_N	functional operator implying propagation of a given state vector along a conic trajectory to the point of entrance into a sphere of given radius
C_t	functional operator implying the propagation of a given state vector along a conic trajectory to a given time (i. e., solution of Kepler's problem)
C_X	functional operator implying propagation of a given state vector along a conic trajectory to the point of exit from a sphere of given radius
G	functional operator implying the conversion of a given selenocentric state vector to geocentric coordinates
G^{-1}	functional operator implying the conversion of a given geocentric state vector to selenocentric coordinates
L_N	functional operator implying linear propagation of a given state vector to the point of entrance into a sphere of given radius
L_t	functional operator implying linear propagation of a given state vector to a given time
L_X	functional operator implying linear propagation of a given state vector to the point of exit from a sphere of given radius
MSI	moon's sphere of influence
N_r	functional operator implying the transformation of a given selenocentric real state vector into a geocentric prepericynthion pseudostate
N_r^{-1}	functional operator implying the transformation of a given geocentric prepericynthion pseudostate into a selenocentric real state vector
N_X	functional operator implying the transformation of a given postpericynthion pseudostate into a prepericynthion pseudostate
PTS	pseudostate transformation sphere
$\vec{R}$	geocentric position vector of spacecraft

NOMENCLATURE (Continued)

Symbol	Definition
$\vec{r}$	selenocentric position vector of spacecraft
r_s	radius of PTS
r_s'	radius of MSI
t	time
$\vec{V}$	geocentric velocity vector of spacecraft
$\vec{v}$	selenocentric velocity vector of spacecraft
X_N	functional operator implying the transformation of a given prepericynthion pseudostate into a postpericynthion pseudostate
X_r	functional operator implying transformation of a given selenocentric real state vector into a geocentric postpericynthion pseudostate
X_r^{-1}	functional operator implying transformation of a given geocentric postpericynthion pseudostate into a selenocentric real state vector
η	true anomaly
μ	gravitational parameter
$\vec{\nu}$	geocentric velocity vector of moon
$\vec{\rho}$	geocentric position vector of moon
Σ	geocentric state vector of spacecraft (has the components t, $\vec{R}$, and $\vec{V}$)
σ	selenocentric state vector of spacecraft (has the components t, $\vec{r}$, and $\vec{v}$)
σ	standard deviation (square root of variance)
Ω	right ascension of ascending node
ω	argument of perigee

NOMENCLATURE (Continued)

Superscripts	Definition
C	state vector resulting from two-body (conic) propagation
*N	prepericynthion pseudostate
*X	postpericynthion pseudostate

Subscripts	
e	earth
m	moon
N	sphere entrance point
X	sphere exit point

1. INTRODUCTION AND SUMMARY

1.1 PROBLEM STATEMENT

Precise determination of a spacecraft trajectory in the earth-moon system requires numerical integration of the differential equations of motion. Since numerical integration is a time-consuming process, two-body (conic) segments are used extensively to approximate three-body motion during preliminary analyses of lunar missions. In the conventional method of approximation, a "moon's sphere of influence" (MSI) is defined. The MSI is centered on, and moves with, the moon. Outside the MSI, lunar gravity is completely ignored, and the spacecraft motion is described by a geocentric conic. Inside the MSI, earth gravity is ignored (except indirectly as it affects the motion of the moon), and the spacecraft motion is described by a selenocentric conic. If a trajectory is propagated into the MSI, the geocentric conic state vector at the entry point is converted to selenocentric coordinates. The converted state vector defines the selenocentric conic that is used to describe all subsequent motion inside the MSI. The elements of the true osculating selenocentric conic (defined by the true instantaneous state vector) are continuously perturbed by the earth; whereas, the patch-conic elements are held fixed. Therefore, there is a cumulative error in the patched-conic state vector as it is propagated into the MSI. This error can be reduced by making the MSI smaller, but only at the expense of increasing a similar error in the geocentric conic state vector. Selection of an MSI radius requires a compromise to minimize the combined error that results from ignoring lunar perturbations on the geocentric conic and earth perturbations on the selenocentric conic. The compromise value of MSI radius usually is somewhere between 9 and 14 earth radii.

1.2 OVERLAPPED CONIC TECHNIQUE

In the overlapped conic technique, a moon-centered "pseudostate transformation sphere" (PTS) is defined. As in the case of the MSI, lunar perturbations of the geocentric conic are ignored outside the PTS, whose

radius is typically about twice as large as the MSI radius. In contrast to the patched conic method, the geocentric conic is extended into the sphere, rather than being terminated at the PTS surface. Instead of defining a region of exclusive lunar influence, the PTS defines a region wherein geocentric conic states are regarded as pseudostates that are related to their real counterparts by a reversible transformation algorithm. As illustrated in Figure 1-1, real prepericynthion states are related to a geocentric prepericynthion conic, and real postpericynthion states are related to a geocentric postpericynthion conic. The pseudostate is discontinuous at the real pericynthion passage time, but the real (transformed) state is continuous at all times, including the PTS entry and exit times.

The transformation of a geocentric prepericynthion pseudostate to its real selenocentric counterpart is a three-step process requiring (1) conversion of the pseudostate from geocentric to selenocentric coordinates, (2) linear propagation of the converted state backward to the PTS surface, and (3) selenocentric conic propagation forward to the original pseudostate time. Transformation of a geocentric postpericynthion pseudostate is similar, except that the direction of propagation is reversed in steps (2) and (3).

To propagate a real selenocentric state vector to another point on the real trajectory, it is necessary first to transform it into a geocentric pseudostate vector. For a prepericynthion state, the required transformation steps are (1) selenocentric conic propagation backward to the PTS surface, (2) linear propagation forward to the original state time, and (3) conversion of the resulting pseudostate from selenocentric to geocent coordinates. The transformation process is identical for a postpericynthion case, except the direction of propagation is reversed in steps (1) and (2). After the appropriate geocentric pseudostate is defined, it is propagated along a geocentric conic to the desired time or position. If the propagated pseudostate lies outside the PTS, it is taken to be a real geocentric state. Otherwise, it is transformed to a real selenocentric state by the process defined in the preceding paragraph.

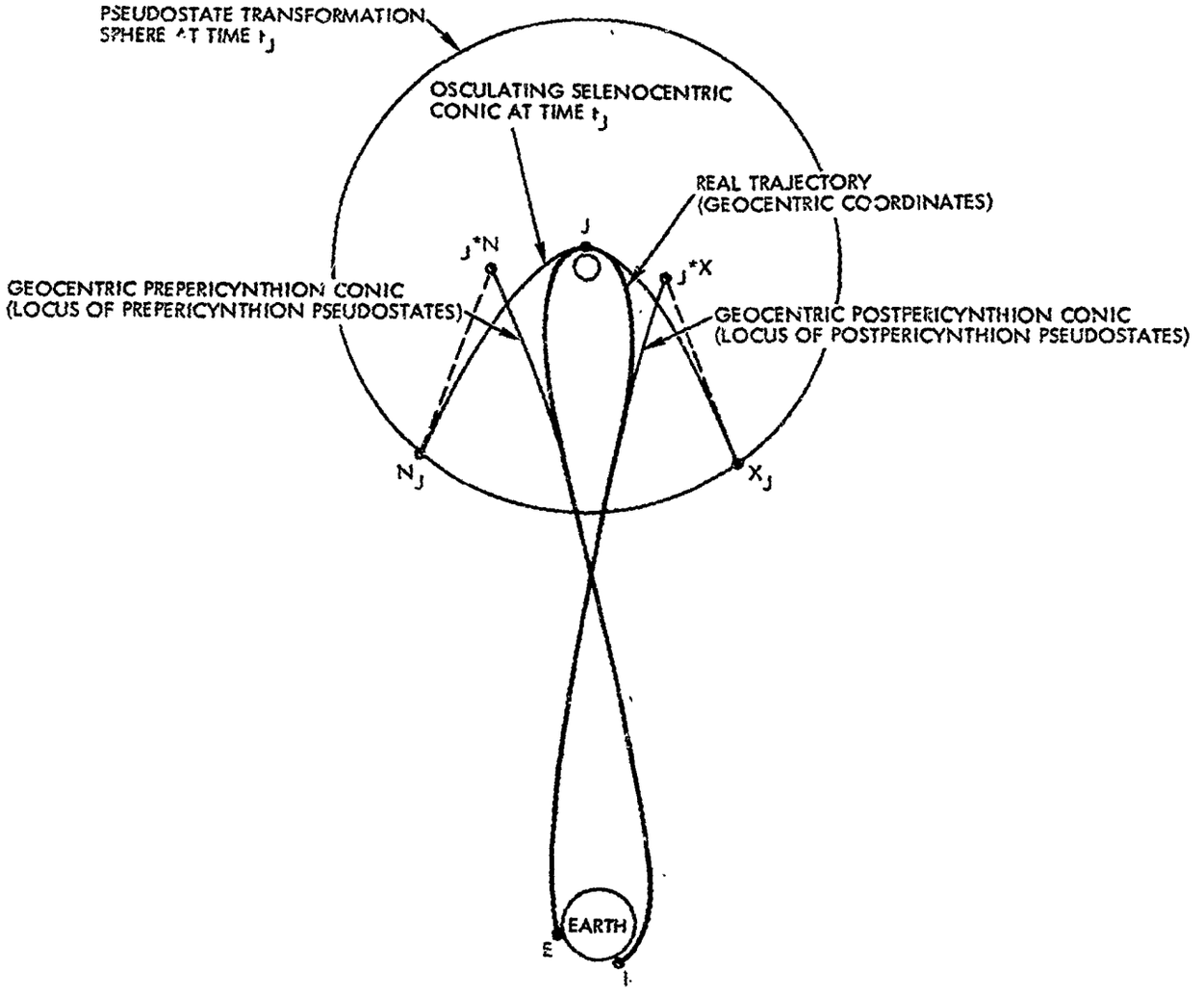

Figure 1-1. Overlapped Conic Simulation of Circumlunar Trajectory

If a real prepericynthion state vector is to be propagated beyond pericynthion to a real postpericynthion state, the geocentric pseudostate must be redefined at or near the real pericynthion passage time. Let t_J be an estimate of the passage time (it does not have to be very accurate, ± one hour is close enough). The original pseudostate is propagated along the geocentric prepericynthion conic to time t_J. Then the propagated pseudostate is (1) converted to selenocentric coordinates, (2) propagated linearly backward to the PTS surface, (3) propagated forward along a selenocentric conic to the PTS surface (i. e., from the hyperbolic entry point to the exit point), (4) propagated linearly backward to time t_J, and (5) converted back to geocentric coordinates. The redefined pseudostate lies on the geocentric postpericynthion conic, and the geocentric propagation of the pseudostate is continued from this point.

Trajectory approximations that result from applying the pseudostate theory summarized in the preceding four paragraphs are referred to as "overlapped conics." This terminology is adopted because geocentric and selenocentric conic segments are overlapped within the PTS, in the sense that the geocentric and the selenocentric two-body differential equations of motion are integrated separately, but over identical time intervals.

The overlapped conic technique affords a better dynamic simulation of three-body motion than the patched conic technique and yields errors only about 20 percent as great (in the case of lunar missions) as corresponding patched conic errors. Execution time and adaptability to split boundary value problems are generally comparable, and in some cases the overlapped conic technique is superior to the patched conic method in both respects. The overlapped conic simulation can be incorporated into existing patched conic computer programs with only minor changes in coding; therefore, rapid implementation of the overlapped conic technique is possible.

Although derived specifically for the simulation of lunar missions, the general pseudostate theory (upon which the overlapped conic method is based) is applicable to any three-body system in which the tertiary body has negligible mass and hyperbolic energy relative to the secondary body,

provided the mass of the primary body is quite large relative to the mass of the secondary body. It is believed, therefore, that the overlapped conic technique can be applied to interplanetary trajectories. An empirical determination of the optimum PTS radius would be required for each planet involved.

The theory described in this document represents an extension and a generalization of the basic transformation algorithm described in Reference 1. The transformation equations presented are derived from basic theoretical considerations; whereas, the derivation in Reference 1 was based primarily an intuitive logic.

2. DERIVATION OF EQUATIONS

2.1 EQUATIONS OF EARTH-RELATIVE MOTION

If all forces except the central gravitational forces of the earth and the moon are ignored, the earth-relative motion of a spacecraft in the earth-moon system is governed by the three-body differential equation

$$\ddot{\vec{R}} = -\mu_e \vec{R}/R^3 - \mu_m \vec{r}/r^3 - \mu_m \vec{\rho}/\rho^3, \tag{1}$$

where the inertial position vectors $\vec{R}$, $\vec{r}$, and $\vec{\rho}$ are defined in Figure 2-1.

2.1.1 True Earth-Relative Trajectory

Given an initial geocentric state vector

$$\Sigma_I = \left(t_I, \vec{R}_I, \vec{V}_I\right), \tag{2}$$

the velocity and position components of any other true state vector

$$\Sigma_J = \left(t_J, \vec{R}_J, \vec{V}_J\right) \tag{3}$$

on the same trajectory are defined by the integral equations

$$\vec{V}_J = \int_{t_I}^{t_J}\left(-\mu_e \vec{R}/R^3\right)dt + \int_{t_I}^{t_J}\left(-\mu_m \vec{r}/r^3\right)dt + \int_{t_I}^{t_J}\left(-\mu_m \vec{\rho}/\rho^3\right)dt + \vec{V}_I \tag{4}$$

and

$$\vec{R}_J = \int_{t_I}^{t_J}\int_{t_I}^{t}\left(-\mu_e \vec{R}/R^3\right)dt\,dt + \int_{t_I}^{t_J}\int_{t_I}^{t}\left(-\mu_m \vec{r}/r^3\right)dt\,dt$$

$$+ \int_{t_I}^{t_J}\int_{t_I}^{t}\left(-\mu_m \vec{\rho}/\rho^3\right)dt\,dt + \left(t_J - t_I\right)\vec{V}_I + \vec{R}_I\,. \tag{5}$$

There are no known general closed-form solutions for the first two terms in Equations (4) and (5); therefore, numerical integration is required to define the spacecraft trajectory accurately.

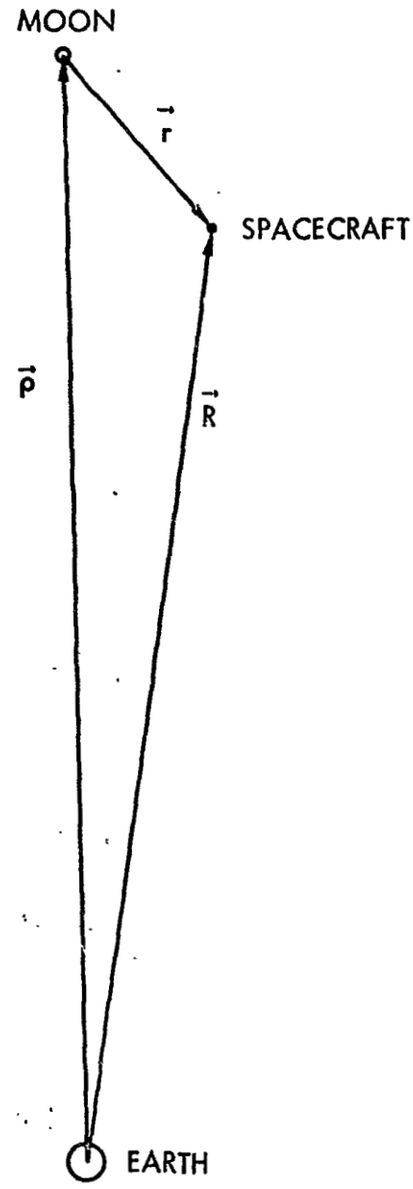

Figure 2-1. Vector Position Diagram

2. 1. 2 Geocentric Conic Trajectory

The sum of the last two terms in Equation (1) is very small when the spacecraft is very near the earth. If the spacecraft is near the earth throughout the time interval of interest, its motion can be assumed to be governed by the two-body differential equation

$$\ddot{\vec{R}}^c = -\mu_e \vec{R}^c / \left(R^c\right)^3 , \tag{6}$$

and the conic state vector

$$\Sigma_J^c = \left(t_J, \vec{R}_J^c, \vec{V}_J^c\right) \tag{7}$$

can be assumed to be a good estimate of the true state vector Σ_J.

The conic velocity and position vectors $\vec{V}_J^c$ and $\vec{R}_J^c$ (obtained from closed-form equations) represent the integral solutions

$$\vec{V}_J^c = \int_{t_I}^{t_J} \left[-\mu_e \vec{R}^c / (R^c)^3\right] dt + \vec{V}_I \tag{8}$$

and

$$\vec{R}_J^c = \int_{t_I}^{t_J} \int_{t_I}^{t} \left[-\mu_e \vec{R}^c / (R^c)^3\right] dt\, dt + \left(t_J - t_I\right) \vec{V}_I + \vec{R}_I , \tag{9}$$

of Equation (6).

2. 2 EQUATIONS OF MOON-RELATIVE MOTION

The moon-relative motion of the spacecraft (again, ignoring all forces other than the central gravitational forces of the earth and the moon) is governed by the differential equation

$$\ddot{\vec{r}} = -\mu_m \vec{r}/r^3 - \mu_e \vec{R}/R^3 + \mu_e \vec{\rho}/\rho^3 . \tag{10}$$

Equation (10) is no more and no less correct than Equation (1); however, it is often more convenient to use when the spacecraft is near the moon.

2. 2. 1 True Moon-Relative Trajectory

Given an initial selenocentric state vector

$$\sigma_I = \left(t_I, \vec{r}_I, \vec{v}_I\right) , \tag{11}$$

the velocity and position components of the true state vector

$$\sigma_J = \left(t_J, \vec{r}_J, \vec{v}_J\right) \tag{12}$$

are defined by the integral equation

$$\vec{v}_J = \int_{t_I}^{t_J}\left(-\mu_m \vec{r}/r^3\right)dt + \int_{t_I}^{t_J}\left(-\mu_e \vec{R}/R^3\right)dt + \int_{t_I}^{t_J}\left(\mu_e \vec{\rho}/\rho^3\right)dt + \vec{v}_I \tag{13}$$

and

$$\vec{r}_J = \int_{t_I}^{t_J}\int_{t_I}^{t}\left(-\mu_m \vec{r}/r^3\right)dt\,dt + \int_{t_I}^{t_J}\int_{t_I}^{t}\left(-\mu_e \vec{R}/R^3\right)dt\,dt$$

$$+ \int_{t_I}^{t_J}\int_{t_I}^{t}\left(\mu_e \vec{\rho}/\rho^3\right)dt\,dt + \left(t_J - t_I\right)\vec{v}_I + \vec{r}_I . \tag{14}$$

Again, numerical integration is necessary to define an accurate moon-relative trajectory, because there are no known general closed-form solutions for the first two terms in Equation (13) and in Equation (14).

2. 2. 2 Selenocentric Conic Trajectory

When the spacecraft is very near the moon, the sum of the last two terms in Equation (10) is very small. If the spacecraft stays near the moon throughout the time interval of interest, its motion can be assumed to be governed by the two-body differential equation

$$\ddot{\vec{r}}^{\,c} = -\mu_m \vec{r}^{\,c}/\left(r^c\right)^3 , \tag{15}$$

and the conic state vector

$$\sigma_J^c = \left(t_J,\ \vec{r}_J^c,\ \vec{v}_J^c\right) \tag{16}$$

can be assumed to be a good estimate of the true state vector σ_J.

The conic velocity and position vectors $\vec{v}_J^c$ and $\vec{r}_J^c$ represent the integral solutions,

$$\vec{v}_J^c = \int_{t_I}^{t_J} \left[-\mu_m \vec{r}^c/(r^c)^3\right] dt + \vec{v}_I \tag{17}$$

and

$$\vec{r}_J^c = \int_{t_I}^{t_J} \int_{t_I}^{t} \left[-\mu_m \vec{r}^c/(r^c)^3\right] dt\, dt + \left(t_J - t_I\right)\vec{v}_I + \vec{r}_I\ , \tag{18}$$

of the differential equation (15).

2.3 OVERLAPPED CONIC APPROXIMATION OF A TRANSEARTH TRAJECTORY

Given the selenocentric state vector

$$\sigma_I = \left(t_I,\ \vec{r}_I,\ \vec{v}_I\right) \tag{19}$$

of a spacecraft initially near the moon, assume it is required to calculate an estimate of the geocentric state vector

$$\Sigma_K = \left(t_K,\ \vec{R}_K,\ \vec{V}_K\right) \tag{20}$$

on the earth approach trajectory at a given geocentric distance R_K, where $R_K = \left|\vec{R}_K\right| << \rho_K$. Neither Equation (6) nor Equation (15) is valid over the entire trajectory. However, Equation (6) is reasonably accurate for describing the motion of the spacecraft after the selenocentric distance r becomes greater than some (as yet, undetermined) distance r_s. Therefore, it will be attempted to derive an accurate approximation

$$\Sigma_X^{*X} = \left(t_X,\ \vec{R}_X^{*X},\ \vec{V}_X^{*X}\right) \tag{21}$$

of the spacecraft's true geocentric state vector Σ_X at the time of exit from a selenocentric sphere of radius r_s. This state vector can then be propagated along a geocentric conic to the desired geocentric distance R_K. The selenocentric sphere defined by r_s will be called (for reasons to be explained later) the "pseudostate transformation sphere" (PTS).

The evaluation of Σ_X^{*X} will be accomplished by approximate integration of the three-body differential equation (1). The problem of integration will be simplified by ignoring the third term in Equation (1). The third term can be integrated quite easily in closed form; therefore, its omission is not absolutely necessary for purposes of mathematical simplification. However, its magnitude is quite small relative to the magnitudes of the first two terms, and its omission usually does not have a very great effect on the accuracy of the solution. For "reasonable" lunar mission trajectories (i. e., those in which the spacecraft approaches the moon from the direction of the earth and departs in the direction of the earth), omission of the third term tends to compensate for inaccuracies in the approximate integration of the first two terms, thereby actually increasing the accuracy of the solution.

2. 3. 1 Incomplete Evaluation of PTS Exit Velocity Vector

The velocity component of Σ_X^{*X} is given by

$$\vec{V}_X^{*X} \cong \int_{t_I}^{t_X} \left(-\mu_e \vec{R}/R^3\right) dt + \int_{t_I}^{t_X} \left(-\mu_m \vec{r}/r^3\right) dt + \vec{V}_I \ . \tag{22}$$

It is assumed that the geocentric position and velocity vectors of the moon at time t_I (or any other time) are available from a lunar ephemeris. Therefore, the last term in Equation (22) can be found merely by converting the initial selenocentric velocity vector to geocentric coordinates, thus

$$\vec{V}_I = \vec{v}_I + \vec{v}_I \ . \tag{23}$$

An approximate value for the second term in Equation (22) can be found by considering Equation (17). Inside the PTS (if its radius r_s is not too large), the selenocentric conic position vector $\vec{r}^c$ (defined by conic propagation of the initial selenocentric state vector σ_I) is approximately equal to the true position vector $\vec{r}$. Therefore,

$$\int_{t_I}^{t_X} \left(-\mu_m \vec{r}/r^3\right) dt \cong \vec{v}_X^c - \vec{v}_I \ , \tag{24}$$

where $\vec{v}_X^c$ is the velocity component of the state vector

$$\sigma_X^c = \left(t_X,\ \vec{r}_X^c,\ \vec{v}_X^c\right) \tag{25}$$

defined by

$$\sigma_X^c = C_X\left(\mu_m,\ \sigma_I,\ r_s\right) \ . \tag{26}$$

The functional operator C_X implies propagation of the initial state vector σ_I along a selenocentric conic to the point of exit from a sphere of radius r_s.

Substitution of (24) and (23) into (22) yields

$$\vec{V}_X^{*X} \cong \int_{t_I}^{t_X} \left(-\mu_e \vec{R}/R^3\right) dt + \vec{V}_I^{*X} \ , \tag{27}$$

where

$$\vec{V}_I^{*X} \equiv \vec{v}_I + \vec{v}_X^c \ . \tag{28}$$

The evaluation of $\vec{V}_X^{*X}$, incomplete because a closed-form expression for the integral $\int_{t_I}^{t_X} \left(-\mu_e \vec{R}/R^3\right) dt$ appearing in (27) has not yet been derived. Complete evaluation of $\vec{V}_X^{*X}$ will be deferred until after a partial evaluation of the PTS exit position vector $\vec{R}_X^{*X}$ has been accomplished.

2.3.2 Incomplete Evaluation of PTS Exit Position Vector

The position component of Σ_X^{*X} is given by

$$\vec{R}_X^{*X} \cong \int_{t_I}^{t_X}\int_{t_I}^{t}\left(-\mu_e \vec{R}/R^3\right)dt\,dt + \int_{t_I}^{t_X}\int_{t_I}^{t}\left(-\mu_m \vec{r}/r^3\right)dt\,dt$$

$$+ \left(t_X - t_I\right)\vec{V}_I + \vec{R}_I \,. \tag{29}$$

The initial geocentric position vector is given by

$$\vec{R}_I = \vec{\rho}_I + \vec{r}_I, \tag{30}$$

and the initial geocentric velocity vector $\vec{V}_I$ has already been defined by Equation (23).

An approximation of the second term in Equation (29) is found by considering the selenocentric conic equation (18). Again because the selenocentric conic position vector $\vec{r}^c$ is a good approximation of the true position vector $\vec{r}$ inside the PTS,

$$\int_{t_I}^{t_X}\int_{t_I}^{t}\left(-\mu_m \vec{r}/r^3\right)dt\,dt \cong \left(\vec{r}_X^c - \vec{r}_I\right) - \left(t_X - t_I\right)\vec{v}_I \,. \tag{31}$$

When (31), (30), and (23) are substituted into (29),

$$\vec{R}_X^{*X} \cong \int_{t_I}^{t_X}\int_{t_I}^{t}\left(-\mu_e \vec{R}/R^3\right)dt\,dt + \left(t_X - t_I\right)\vec{V}_I^{*X} + \vec{R}_I^{*X} \,, \tag{32}$$

where $\vec{V}_I^{*X}$ has already been defined by Equation (28), and where

$$\vec{R}_I^{*X} \equiv \vec{\rho}_I + \left[\vec{r}_X^c - \left(t_X - t_I\right)\vec{v}_X^c\right]. \tag{33}$$

The quantities t_X, $\vec{r}_X^c$, and $\vec{v}_X^c$ are components of the state vector σ_X^c defined by (26).

2.3.3 The Pseudostate Propagation Hypothesis

Comparison of the approximate integral equations (which were derived earlier and are repeated here for convenience) describing the PTS exit velocity and position vector

$$\vec{V}_X^{*X} \cong \int_{t_I}^{t_X} \left(-\mu_e \vec{R}/R^3\right) dt + \vec{V}_I^{*X} \tag{27}$$

$$\vec{R}_X^{*X} \cong \int_{t_I}^{t_X} \int_{t_I}^{t} \left(-\mu_e \vec{R}/R^3\right) dt\, dt + \left(t_X - t_I\right) \vec{V}_I^{*X} + \vec{R}_I^{*X} \tag{32}$$

with the integral equations describing state vector propagation along a geocentric conic trajectory

$$\vec{V}_J^{c} = \int_{t_I}^{t_J} \left[-\mu_e \vec{R}^c/(R^c)^3\right] dt + \vec{V}_I \tag{8}$$

$$\vec{R}_J^{c} = \int_{t_I}^{t_J} \int_{t_I}^{t} \left[-\mu_e \vec{R}^c/(R^c)^3\right] dt\, dt + \left(t_J - t_I\right) \vec{V}_I + \vec{R}_I \tag{9}$$

suggests, as a hypothesis, that the operation

$$\Sigma_X^{*X} = C_t\left(\mu_e,\ \Sigma_I^{*X},\ t_X\right) \tag{34}$$

would yield a good approximation of the true PTS exit state vector Σ_X. In (34), the functional operator C_t implies propagation of the initial "pseudostate" vector

$$\Sigma_I^{*X} \equiv \left(t_I,\ \vec{R}_I^{*X},\ \vec{V}_I^{*X}\right) \tag{35}$$

along a geocentric conic trajectory to the given time t_X.

If this hypothesis is correct, then the desired estimate of the true geocentric state vector Σ_K can be obtained by

$$\Sigma_K^{*X} = C_N\left(\mu_e,\ \Sigma_X^{*X},\ R_K\right) , \tag{36}$$

where the functional operator C_N here implies propagation of Σ_X^{*X} along a geocentric conic to the point of entry into a geocentric sphere of radius R_K. It is not necessary to actually calculate Σ_X^{*X} to solve the example problem. The sequential operations implied by (34) and (36) can be replaced by the single operation

$$\Sigma_K^{*X} = C_N\left(\mu_e,\ \Sigma_I^{*X},\ R_K\right) , \tag{37}$$

which yields precisely the same final state vector with much less computation effort.

The validity of the pseudostate propagation hypothesis depends on how closely the geocentric pseudostate position vector $\vec{R}^{*X}$ (as defined by the geocentric conic propagation of Σ_I^{*X}) agrees with the true position vector $\vec{R}$ between times t_I and t_X. Ultimately, the hypothesis must be validated by empirical results. However, some insight as to the probable range of validity can be obtained from a qualitative analysis of the difference between real and pseudostate positions at the initial state time t_I. This can best be accomplished by converting the geocentric pseudostate to selenocentric coordinates, yielding

$$\sigma_I^{*X} = \left(t_I,\ \vec{r}_I^{*X},\ \vec{v}_I^{*X}\right) , \tag{38}$$

where

$$\vec{r}_I^{*X} = \vec{r}_X^{c} - \left(t_X - t_I\right)\vec{v}_X^{c} \tag{39}$$

and

$$\vec{v}_I^{*X} = \vec{v}_X^{c} . \tag{40}$$

Equations (39) and (40) result from subtracting the geocentric position and velocity vectors of the moon from $\vec{R}_I^{*X}$ and $\vec{V}_I^{*X}$, as defined in Equations (33) and (28), respectively.

Equations (39) and (40) imply that σ_I^{*X} is obtained simply by a linear propagation of σ_X^c (which was obtained by propagating σ_I along a selenocentric conic to the PTS exit point) backward to the original state time t_I. This linear propagation can be described by using the functional notation

$$\sigma_I^{*X} = L_t\left(\sigma_X^c,\ t_I\right) , \tag{41}$$

which implies the operations described in (39) and (40).

In selenocentric coordinates, the pseudostate position lies on a straight line that is tangent, at the PTS exit point, to the osculating selenocentric hyperbola defined by σ_I. The distance from the PTS surface to the pseudostate position is equal to $\left|\left(t_X - t_I\right)\vec{v}_X^c\right|$.

Figure 2-2 illustrates schematically the pseudostate position for five different positions of the real initial state. It is apparent that as $\left(t_X - t_I\right)$ increases, the distance between the real initial position I and the pseudostate initial position I^{*X} increases. In particular, the pseudostate initial positions I_4^{*X} and I_5^{*X} differ considerably from their real counterparts I_4 and I_5, which lie on the prepericynthion leg of the osculating hyperbola. Because of the significant divergence of the pseudostate position from its real counterpart on the prepericynthion leg, the propagation of the geocentric pseudostates $\Sigma_{I_4}^{*X}$ or $\Sigma_{I_5}^{*X}$ along a geocentric conic can not be expected to yield an accurate approximation of the true PTS exit state vector Σ_X.

The pseudostate propagation hypothesis can be extended to cover prepericynthion cases. However, the extended hypothesis involves the use of a prepericynthion geocentric pseudostate Σ_I^{*N} (as distinguished from the postpericynthion geocentric pseudostate Σ_I^{*X}) which has not yet been defined. It will be helpful to explore some of the implications of the pseudostate propagation hypothesis, as applied strictly to postpericynthion states, before proceeding with the extension of the hypothesis to prepericynthion cases. Therefore, the prepericynthion pseudostate definition will be deferred temporarily.

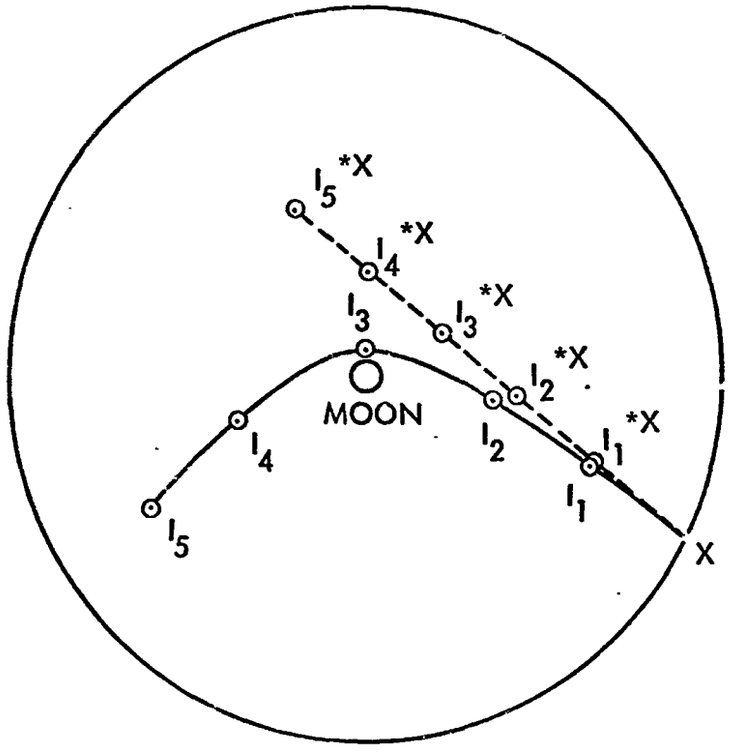

Figure 2-2. Relation Between Real Position and Postpericynthion Pseudostate Position (Selenocentric Coordinates)

2.3.4 Implications of the Propagation Hypothesis

If the pseudostate propagation hypothesis described in the previous section is valid in general for solutions of the type of problem given as an example (i.e., for estimation of a geocentric state vector Σ_K located outside the PTS, given any real postpericynthion state vector σ_I i e the PTS), then by implication it is valid for the propagation of any post-pericynthion state vector to any point (inside or outside the PT S, the same real postpericynthion trajectory. The reasoning is straighforward: if the same estimate of Σ_K is obtained for any true state vector σ_I (where $t_I < t_X$) on a given real postpericynthion trajectory, the geocentric conic along which the pseudostates are propagated must be unique. Furthermore, there must be a one-to-one correspondence between the real state vectors and the pseudostates defined by the geocentric conic.

Now, if real postpericynthion state vectors are related to pseudostates on a unique geocentric postpericynthion conic by a one-to-one transformation algorithm, then it follows that real prepercynthion state vectors must be related (by a similar algorithm) to pseudostates on a geocentric prepericynthion conic. The nature of the prepericynthion transformation can be deduced from a mathematical derivation similar to that contained in Sections 2.3.1 through 2.3.3, or more easily by studying the geometrical aspects of the postpericynthion transformation and applying the basic principles to the prepericynthion case. The geometrical properties of the prepericynthion transformation are illustrated in Figure 2-3, which is the prepericynthion analogue of Figure 2-2.

2.4 THE PSEUDOSTATE THEORY

The following subsections define a pseudostate theory for approximating the three-body trajectory of a spacecraft in the earth-moon system. It is assumed that the energy of the spacecraft is hyperbolic with respect to the moon.

The theory is a formal statement of logical inferences drawn from the analysis presented in Section 2.3. It is based on the assumption that the pseudostate propagation hypothesis described in Section 2.3.3 is valid.

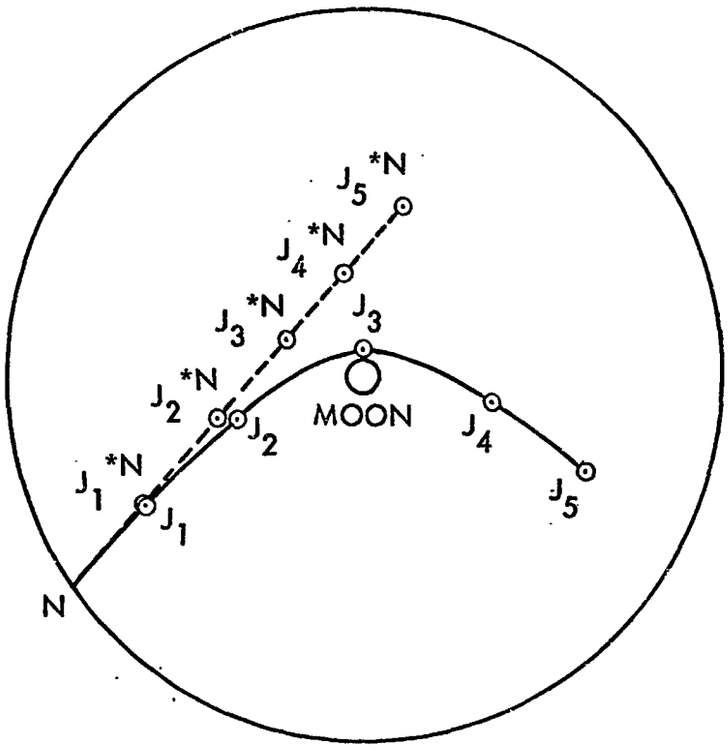

Figure 2-3. Relation Between Real Position and Prepericynthion Pseudostate Position (Selenocentric Coordinates)

The definition of the theory is made prior to the validation of the underlying assumption, because the ultimate validation rests on empirical data generated by application of the theory.

The six transformation functions required for application of the pseudostate theory to state vector propagation problems are defined in Appendixes C, D, and E. These six functions are described by use of the lower-order function definitions contained in Appendixes A and B.

The theory is defined specifically as it applies to the motion of a spacecraft in the earth-moon system. However, it is applicable to the motion of any tertiary body in any three-body system, provided the tertiary body has negligible mass and hyperbolic energy relative to the secondary body, and provided the mass of the secondary body is quite small relative to the mass of the primary body.

2.4.1 The Pseudostate Transformation Sphere

The earth-moon system is divided into two regions separated by the surface of a pseudostate transformation sphere (PTS). The PTS is centered on and moves with the moon. From analytical considerations, the optimum radius of the PTS is expected to be approximately half the mean geocentric distance of the moon; the exact radius is to be determined empirically.

2.4.2 Pseudostate Vectors

For every real spacecraft state vector, there exists one or two pseudostate vectors. Outside the PTS, there is a one-to-one correspondence between real states and pseudostates; specifically, the geocentric pseudostate is identically equal to its real counterpart.

Inside the PTS, every real state is related, (1) to a unique prepericynthion pseudostate by a reversible prepericynthion pseudostate transformation algorithm, and (2) to a unique postpericynthion pseudostate by a reversible postpericynthion pseudostate transformation algorithm.

2.4.3 Loci of Pseudostate Vectors

For a given real spacecraft trajectory, there exist two unique geocentric conic trajectories:

1) A prepericynthion geocentric conic, which is the locus of geocentric prepericynthion pseudostates

2) A postpericynthion geocentric conic, which is the locus of geocentric postpericynthion pseudostates

2.4.4 State Vector Propagation

If any real state vector is to be propagated over a given interval of time to define another state vector on the real trajectory, it must first be transformed into a geocentric pseudostate and then propagated along the appropriate geocentric conic for the same interval of time. The propagated real state vector is obtained by performing a pseudostate-to-real transformation of the propagated pseudostate.

Real prepericynthion state vectors are defined by propagating the prepericynthion pseudostate along the geocentric prepericynthion conic, and real postpericynthion state vectors are defined by propagating the postpericynthion pseudostate along the geocentric postpericynthion conic. If it is necessary to propagate a pseudostate beyond the real pericynthion passage time, the pseudostate must be redefined (i. e., transformed from a prepericynthion pseudostate to a postpericynthion pseudostate, or vice versa) at or near the time of real pericynthion passage.

3. EMPIRICAL VALIDATION

To test the pseudostate propagation hypothesis of Section 2. 3. 3 (and the pseudostate theory derived from it), overlapped conic transearth trajectories were computed for a set of real selenocentric initial state vectors. As indicated in Figure 3-1, the total flight time to perigee ranged from approximately 27 hours to 167 hours. State vectors defining selenocentric posigrade and selenocentric retrograde motion were included in the test set. Pericynthion altitudes ranged from near zero to approximately 4 earth radii.

A few (about half a dozen) representative cases were selected initially to be used for an empirical determination of a suitable value for the PTS radius. Based on this preliminary investigation, a value of $r_s = 24$ earth radii was selected, and this value was used in all subsequent overlapped conic trajectory computations. This is not an optimum value for all lunar mission simulations (Reference 2), but it appears to give very good results for a wide range of transearth trajectories.

After fixing the PTS radius at 24 earth radii, overlapped conic propagation errors in several geocentric trajectory parameters (judged to be most significant in transearth trajectory simulations) were determined for each test case. These errors are plotted in Figures 3-2 through 3-5, along with errors resulting from competitive methods of three-body trajectory approximation. All errors in these figures are measured relative to precision values obtained from a highly accurate computer program that numerically integrates the perturbing accelerations arising from earth oblateness and solar gravitational influence, as well as the central gravitational accelerations of the earth and the moon. The numerical integrations were repeated, with earth oblateness and solar perturbations zeroed out, in a limited number of cases. This was done to obtain estimates (the lowermost dashed curves in Figures 3-2 through 3-5) of the effects of earth oblateness and solar perturbations on the total propagation error.

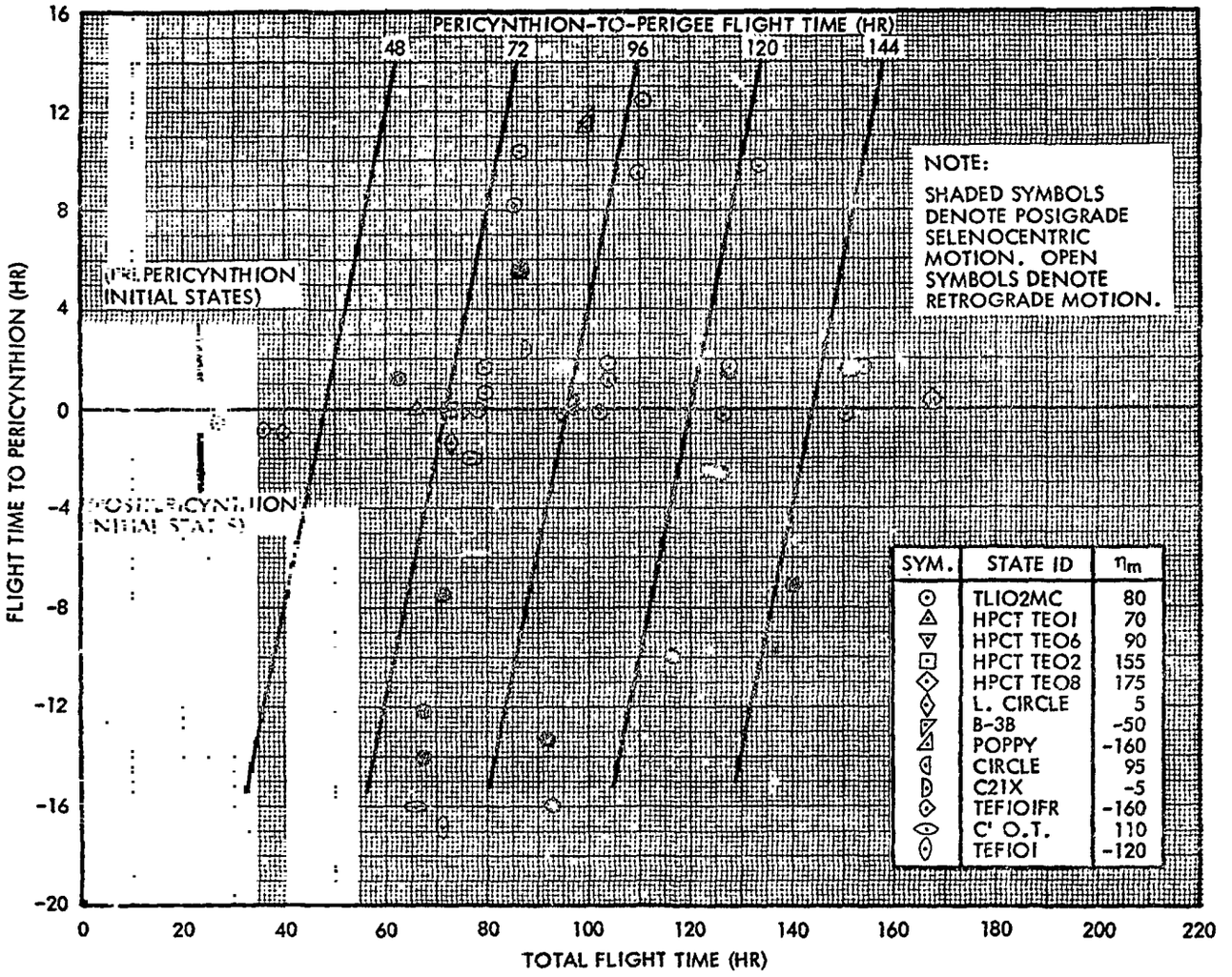

Figure 3-1. Overlapped Conic Transearth Test Cases

As indicated in Figures 3-2 through 3-5, the overlapped conic errors are generally only about 20 percent as great as corresponding patched conic errors. (Approximately the same degree of improvement has been documented, for translunar cases and a fixed PTS radius, in Reference 3.) This is felt to be extremely significant, because the overlapped conic method and the patched conic method are comparable in terms of execution time and their adaptability to the solution of split boundary value problems. (In some cases, the overlapped conic is superior in both respects.) The necessary computations are also very similar, which means that only minor coding changes are required to incorporate the overlapped conic model into existing patched conic trajectory computer programs.

Relative to the Jacobi calibration of conventional patched conics, (as implemented in the Moon-Centered Return-to-Earth Program of the Apollo Real Time Computer Complex (RTCC), and as described in Reference 4), the overlapped conic also offers a significant improvement in accuracy. As indicated in Figures 3-3 and 3-5, this is particularly true of flight-time and geocentric inclination errors. The Jacobi calibration, at least as it is implemented in the RTCC, creates a state-vector discontinuity at the conic patch point. This discontinuity, which does not occur in the case of overlapped conic simulation, would be highly unsatisfactory in some applications.

In a few test cases, errors resulting from use of the hybrid patched conic technique (Reference 5) are shown for comparision in Figures 3-2 through 3-5. Although an insufficient number of Hybrid Patched Conic Technique (HPCT) error data points were obtained to justify the estimation of 2σ error limit curves (as was done for the other three-body approxiition methods), the HPCT propagation errors are generally only about one-half to one-third as great as corresponding overlapped conic errors. However, the greater accuracy of the HPCT is expected to be at least partially offset by longer execution time on the average. In any event, the overlapped conic method has a significant advantage over the HPCT in terms of its adaptability to the solution of split boundary value problems.

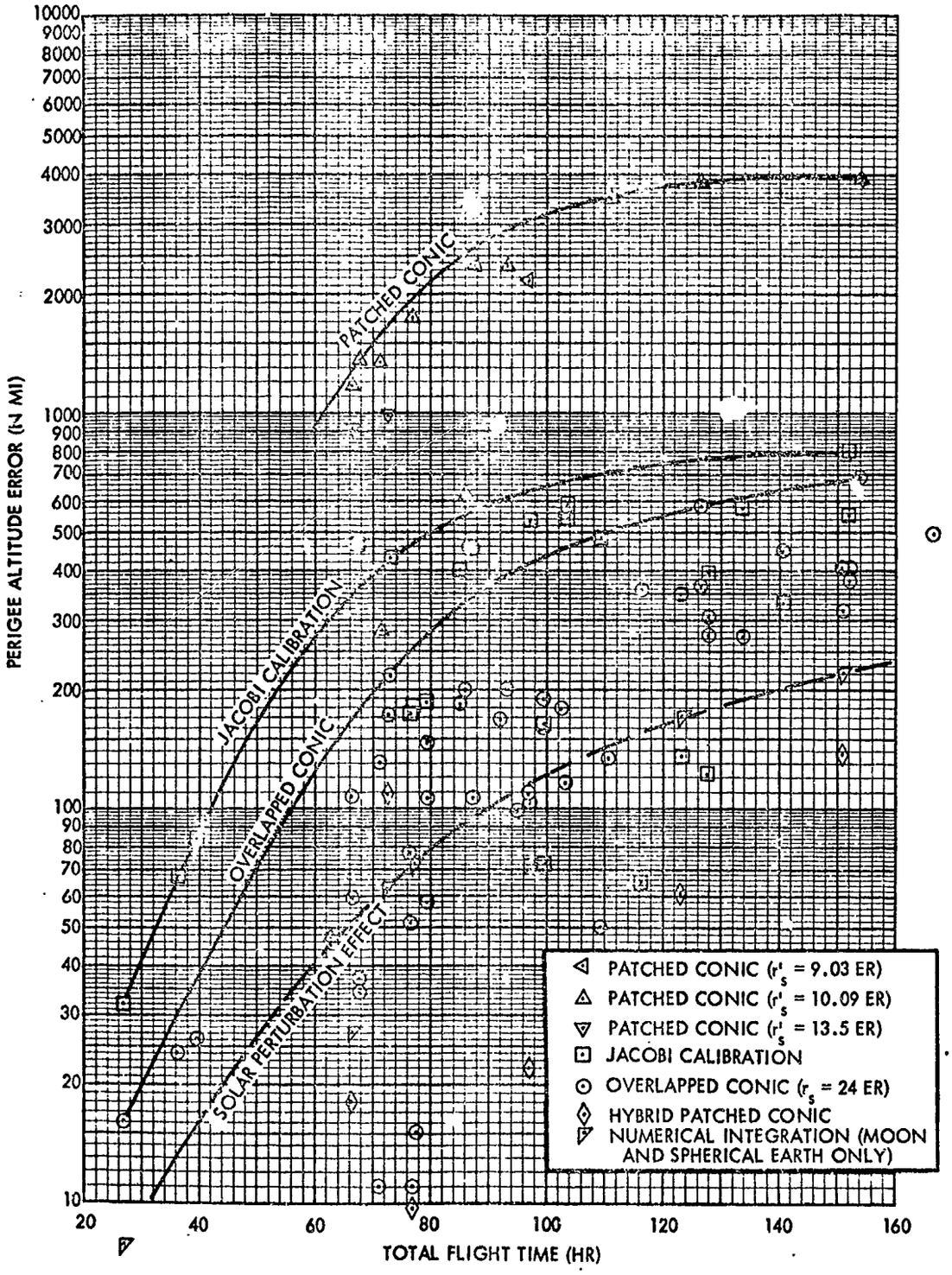

Note: Faired curves represent visually-estimated 2σ error limits. Shaded symbols represent errors greater than $2\sigma_{EST}$.

Figure 3-2. Transearth Perigee Altitude Errors

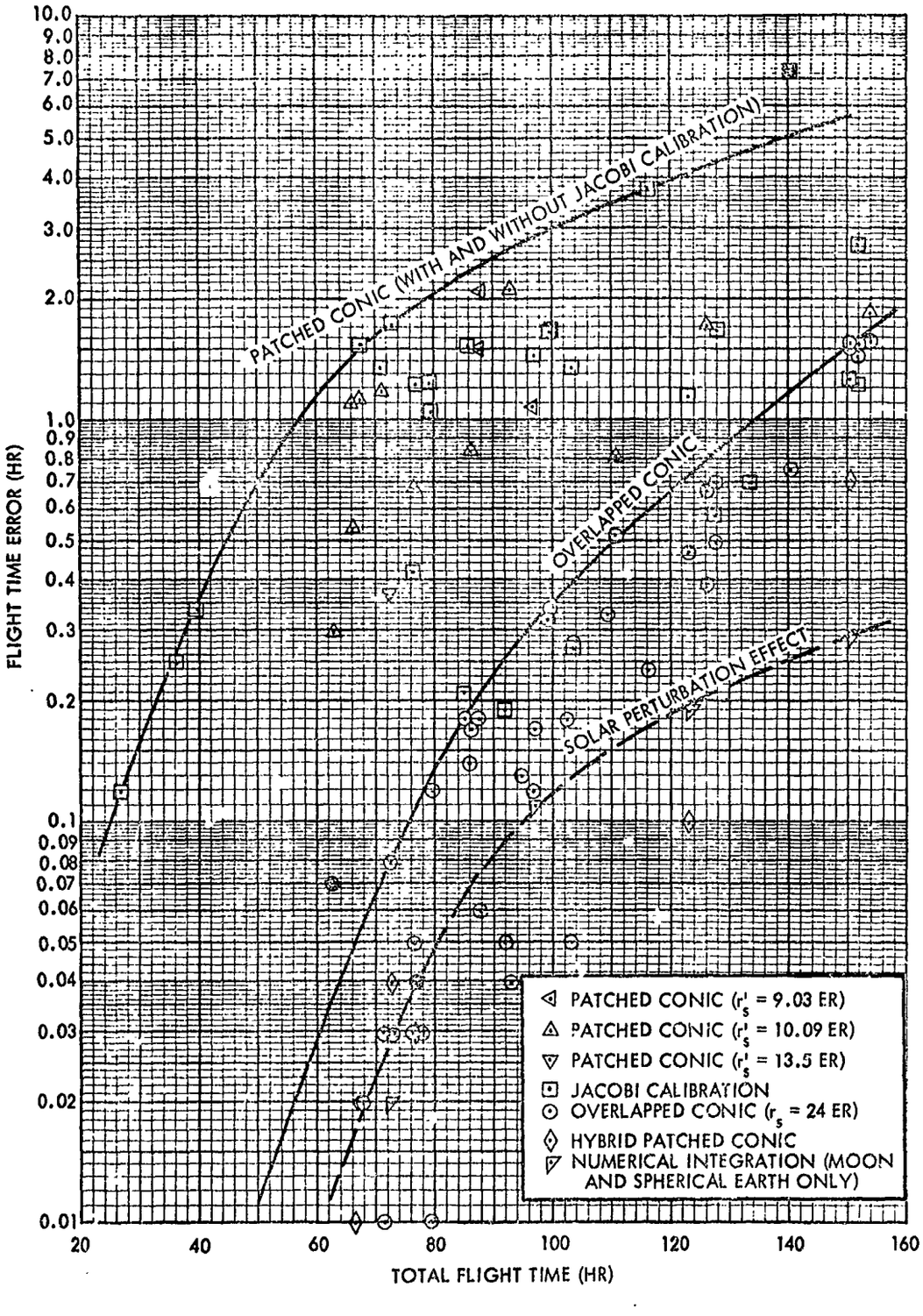

Note: Faired curves represent visually-estimated 2σ error limits. Shaded symbols represent errors greater than $2\sigma_{EST}$

Figure 3-3. Transearth Flight Time Errors

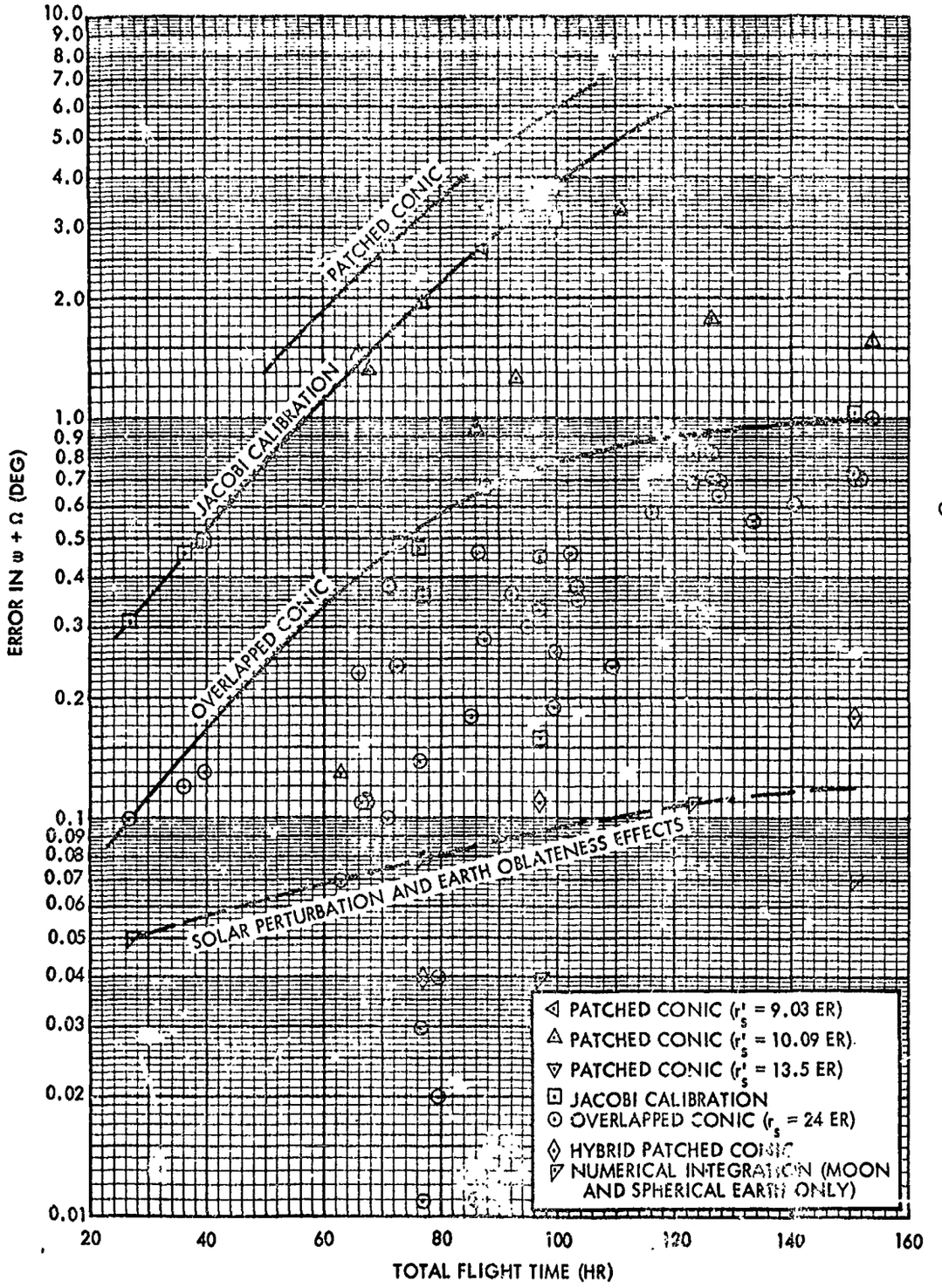

Note: Faired curves represent visually-estimated 2σ error limits. Shaded symbols represent errors greater than $2\sigma_{EST}$.

Figure 3-4. Errors in $(\Omega + \omega)$ of Transearth Geocentric Conic

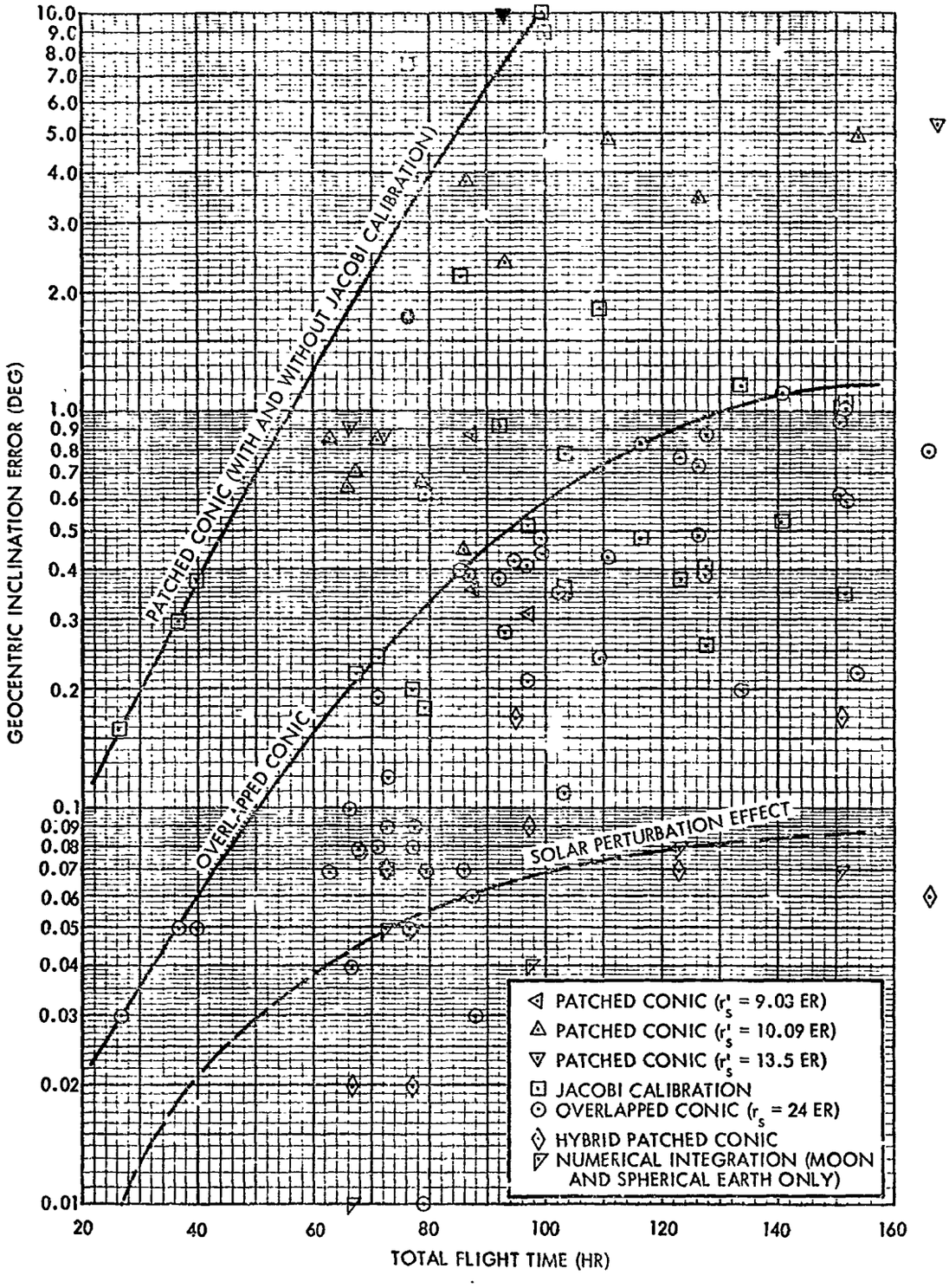

Note: Faired curves represent visually-estimated 2σ error limits. Shaded symbols represent errors greater than $2\sigma_{EST}$.

Figure 3-5. Transearth Geocentric Inclination Errors

The advantage of the overlapped conic model over the patched conic is not limited to improvements in the accuracy of geocentric trajectory parameters. For instance, in the case of prepericynthion initial states, a critical selenocentric trajectory parameter is the predicted pericynthion altitude. When conventional conic approximations are used, the predicted pericynthion altitude is the pericynthion altitude of the osculating selenocentric conic defined by the initial state vector. Since the elements of the osculating conic are continuously perturbed by the earth, an osculating conic prediction can be very inaccurate if it is made several hours before pericynthion passage.

Overlapped conic predictions of pericynthion altitude, for a typical lunar approach trajectory, are compared in Figure 3-6 with the true value and with predictions based on the conventional conic approximation. The accuracy advantage of the overlapped conic method is obvious.

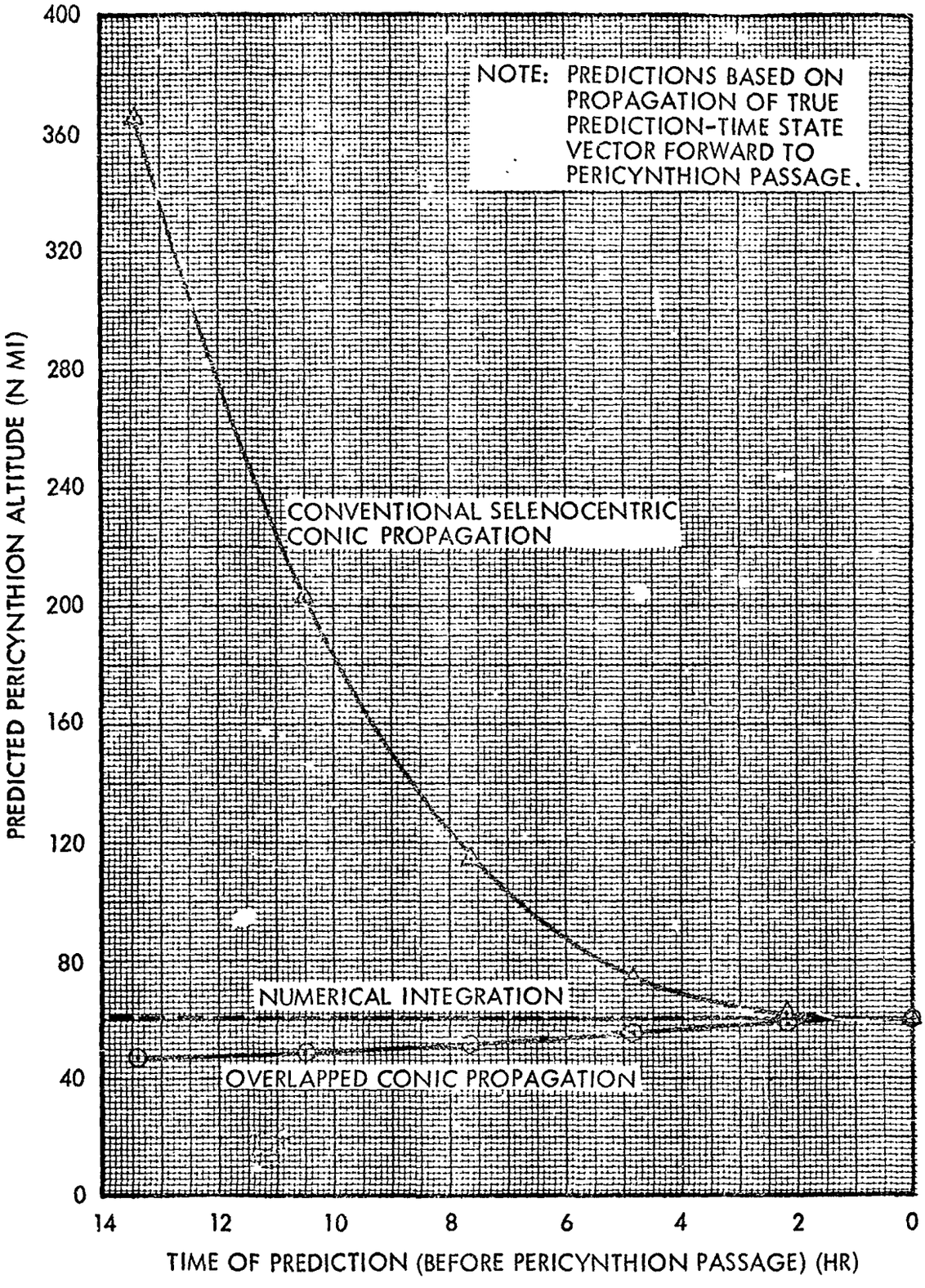

Figure 3-6. Comparison of Pericynthion Altitude Predictions

APPENDIX A

STATE VECTOR CONVERSION FUNCTIONS

A-1 CONVERSION FROM SELENOCENTRIC TO GEOCENTRIC COORDINATES

a) Functional notation: $\Sigma_{\#}^{\dagger} = G\left(\sigma_{\#}^{\dagger}\right)$

b) Input: $\sigma_{\#}^{\dagger} = \left(t_{\#}, \vec{r}_{\#}^{\dagger}, \vec{v}_{\#}^{\dagger}\right)$

c) Output: $\Sigma_{\#}^{\dagger} = \left(t_{\#}, \vec{R}_{\#}^{\dagger}, \vec{V}_{\#}^{\dagger}\right)$

d) Computations:

$$t_{\#} = t_{\#}$$

$$\vec{R}_{\#}^{\dagger} = \vec{r}_{\#}^{\dagger} + \vec{\rho}_{\#}$$

$$\vec{V}_{\#}^{\dagger} = \vec{v}_{\#}^{\dagger} + \vec{\nu}_{\#}$$

e) Comments:

The symbols # and † represent any subscript and superscript.

A-2 CONVERSION FROM GEOCENTRIC TO SELENOCENTRIC COORDINATES

a) Functional notation: $\sigma_{\#}^{\dagger} = G^{-1}\left(\Sigma_{\#}^{\dagger}\right)$

b) Input: $\Sigma_{\#}^{\dagger} = \left(t_{\#}, \vec{R}_{\#}^{\dagger}, \vec{V}_{\#}^{\dagger}\right)$

c) Output: $\sigma_{\#}^{\dagger} = \left(t_{\#}, \vec{r}_{\#}^{\dagger}, \vec{v}_{\#}^{\dagger}\right)$

d) Computations:

$$t_{\#} = t_{\#}$$

$$\vec{r}^{\dagger}_{\#} = \vec{R}^{\dagger}_{\#} - \vec{\rho}_{\#}$$

$$\vec{v}^{\dagger}_{\#} = \vec{V}^{\dagger}_{\#} - \vec{\nu}_{\#}$$

e) Comments:

The symbols # and † represent any subscript and superscript.

APPENDIX B

STATE VECTOR PROPAGATION FUNCTIONS

B-1 LINEAR PROPAGATION TO A SPECIFIED TIME

a) Functional notation: $\sigma_2 = L_t\left(\sigma_1,\ t_2\right)$

b) Input: t_2; $\sigma_1 = \left(t_1,\ \vec{r}_1,\ \vec{v}_1\right)$

c) Output: $\sigma_2 = \left(t_2,\ \vec{r}_2,\ \vec{v}_2\right)$

d) Computations:

$$t_2 = t_2$$

$$\vec{v}_2 = \vec{v}_1$$

$$\vec{r}_2 = \vec{r}_1 + \left(t_2 - t_1\right)\vec{v}_1$$

B-2 LINEAR PROPAGATION TO SPHERE ENTRANCE POINT

a) Functional notation: $\sigma_N = L_N\left(\sigma_1,\ r_s\right)$

b) Input: r_s; $\sigma_1 = \left(t_1,\ \vec{r}_1,\ \vec{v}_1\right)$

c) Output: $\sigma_N = \left(t_N,\ \vec{r}_N,\ \vec{v}_N\right)$

d) Computations:

$$\Delta t = \left[-\left(\vec{r}_1 \cdot \vec{v}_1\right) - \sqrt{\left(\vec{r}_1 \cdot \vec{v}_1\right)^2 + v_1^2\left(r_s^2 - r_1^2\right)}\right] / v_1^2$$

$$t_N = t_1 + \Delta t$$

$$\vec{r}_N = \vec{r}_1 + \Delta t\,\vec{v}_1$$

$$\vec{v}_N = \vec{v}_1$$

e) Comments:

Negative radicand in Δt equation means line does not intersect sphere (possible only when $r_1 > r_s$).

B-3 LINEAR PROPAGATION TO SPHERE EXIT POINT

a) Functional notation: $\sigma_X = L_X\left(\sigma_1, r_s\right)$

b) Input: r_s; $\sigma_1 = \left(t_1, \vec{r}_1, \vec{v}_1\right)$

c) Output: $\sigma_X = \left(t_X, \vec{r}_X, \vec{v}_X\right)$

d) Computations:

$$\Delta t = \left[-\left(\vec{r}_1 \cdot \vec{v}_1\right) + \sqrt{\left(\vec{r}_1 \cdot \vec{v}_1\right)^2 + v_1^2\left(r_s^2 - r_1^2\right)}\right] / v_1^2$$

$$t_X = t_1 + \Delta t$$

$$\vec{r}_X = \vec{r}_1 + \Delta t\, \vec{v}_1$$

$$\vec{v}_X = \vec{v}_1$$

e) Comments:

Negative radicand in Δt equation means line does not intersect sphere (possible only when $r_1 > r_s$).

B-4 CONIC PROPAGATION TO A SPECIFIED TIME

a) Functional notation: $\sigma_2 = C_t\left(\mu, \sigma_1, t_2\right)$

b) Input: μ; t_2; $\sigma_1 = \left(t_1, \vec{r}_1, \vec{v}_1\right)$

c) Output: $\sigma_2 = \left(t_2, \vec{r}_2, \vec{v}_2\right)$

d) Computations:

Solve Kepler's problem to determine two-body state vector at time t_2, given the central body gravitational parameter μ and the state vector at time t_1.

e) Comments:

No explicit solution. Requires iteration. Numerous subroutines available. Selenocentric state symbols used for illustration only (function not restricted to selenocentric state propagation).

B-5 CONIC PROPAGATION TO SPHERE ENTRY POINT

a) Functional notation: $\sigma_N = C_N\left(\mu,\ \sigma_1,\ r_s\right)$

b) Input: μ; r_s; $\sigma_1 = \left(t_1,\ \vec{r}_1,\ \vec{v}_1\right)$

c) Output: $\sigma_N = \left(t_N,\ \vec{r}_N,\ \vec{v}_N\right)$

d) Computations:

Solve explicit two-body equations for t_N, $\vec{r}_N$, and $\vec{v}_N$ at distance r_s, using conic elements defined by μ and σ_1. Impose $\vec{r}_N \cdot \vec{v}_N < 0$ as a condition to get unique solution.

e) Comments:

No solution if conic periapsis distance is greater than r_s, or if apoapsis distance is less than r_s. Selenocentric state symbols used for illustration only (function not restricted to selenocentric state propagation).

B-6 CONIC PROPAGATION TO SPHERE EXIT POINT

a) Functional notation: $\sigma_X = C_X\left(\mu,\ \sigma_1,\ r_s\right)$

b) Input: μ; r_s; $\sigma_1 = \left(t_1,\ \vec{r}_1,\ \vec{v}_1\right)$

c) Output: $\sigma_X = \left(t_X, \vec{r}_X, \vec{v}_X\right)$

d) Computations:

Solve explicit two-body equations for t_X, $\vec{r}_X$, and $\vec{v}_X$ at distance r_s, using conic elements defined by μ and σ_1. Impose $\vec{r}_X \cdot \vec{v}_X > 0$ as a condition to get unique solution.

e) Comments:

No solution if conic periapsis distance is greater than r_s, or if apoapsis distance is less than r_s. Selenocentric state symbols used for illustration only (function not restricted to selenocentric state propagation).

APPENDIX C

REAL-TO-PSEUDOSTATE TRANSFORMATION FUNCTIONS

C-1 PREPERICYNTHION LEG

a) Notation: $\Sigma_I^{*N} = N_r\left(\sigma_I,\ r_s\right)$

b) Input: $r_s;\ \sigma_I = \left(t_I,\ \vec{r}_I,\ \vec{v}_I\right)$

c) Output: $\Sigma_I^{*N} = \left(t_I,\ \vec{R}_I^{*N},\ \vec{V}_I^{*N}\right)$

d) Computations:

$$\sigma_N^c = C_N\left(\mu_m,\ \sigma_I,\ r_s\right)$$

$$\sigma_I^{*N} = L_t\left(\sigma_n^c,\ t_I\right)$$

$$\Sigma_I^{*N} = G\left(\sigma_I^{*N}\right)$$

e) Comments:

Computations shown above apply when $r_I < r_s$.

If $r_I \geq r_s$, then

$$\Sigma_I^{*N} = G\left(\sigma_I\right)$$

C-2 POSTPERICYNTHION LEG

a) Notation: $\Sigma_I^{*X} = X_r\left(\sigma_I,\ r_s\right)$

b) Input: $r_s;\ \sigma_I = \left(t_I,\ \vec{r}_I,\ \vec{v}_I\right)$

c) Output: $\Sigma_I^{*X} = \left(t_I, \vec{R}_I^{*X}, \vec{V}_I^{*X}\right)$

d) Computations:

$$\sigma_X^c = C_X\left(\mu_m, \sigma_I, r_s\right)$$

$$\sigma_I^{*X} = L_t\left(\sigma_X^c, t_I\right)$$

$$\Sigma_I^{*X} = G\left(\sigma_I^{*X}\right)$$

e) Comments:

Computations shown above apply when $r_I < r_s$.

If $r_I \geq r_s$, then

$$\Sigma_I^{*X} = G\left(\sigma_I\right)$$

APPENDIX D

PSEUDOSTATE-TO-REAL TRANSFORMATION FUNCTIONS

D-1 PREPERICYNTHION LEG

a) Notation: $\sigma_K = N_r^{-1}\left(\Sigma_K^{*N},\ r_s\right)$

b) Input: r_s; $\Sigma_K^{*N} = \left(t_K,\ \vec{R}_K^{*N},\ \vec{V}_K^{*N}\right)$

c) Output: $\sigma_K = \left(t_K,\ \vec{r}_K,\ \vec{v}_K\right)$

d) Computations:

$$\sigma_K^{*N} = G^{-1}\left(\Sigma_K^{*N}\right)$$

$$\sigma_N^c = L_N\left(\sigma_K^{*N},\ r_s\right)$$

$$\sigma_K = C_t\left(\mu_m,\ \sigma_N^c,\ t_K\right)$$

e) Comments:

Computations shown above apply when $r_K^{*N} < r_s$.

If $r_K^{*N} \geq r_s$, then

$$\sigma_K = G^{-1}\left(\Sigma_K^{*N}\right)$$

D-2 POSTPERICYNTHION LEG

a) Notation: $\sigma_K = X_r^{-1}\left(\Sigma_K^{*X},\ r_s\right)$

b) Input: r_s; $\Sigma_K^{*X} = \left(t_K,\ \vec{R}_K^{*X},\ \vec{V}_K^{*X}\right)$

c Output: $\sigma_K = \left(t_K, \vec{r}, \vec{v}_K\right)$

d) Computations:

$$\sigma_K^{*X} = G^{-1}\left(\Sigma_K^{*X}\right)$$

$$\sigma_X^c = L_X\left(\sigma_K^{*X}, r_s\right)$$

$$\sigma_K = C_t\left(\mu_m, \sigma_X^c, t_K\right)$$

e) Comments:

Computations shown above apply when $r_K^{*X} < r_s$.

If $r_K^{*X} \geq r_s$, then

$$\sigma_K = G^{-1}\left(\Sigma_K^{*X}\right)$$

APPENDIX E

PSEUDOSTATE-TO-PSEUDOSTATE TRANSFORMATION FUNCTIONS

E-1 PREPERICYNTHION-TO-POSTPERICYNTHION

a) Notation: $\Sigma_J^{*X} = X_N\left(\Sigma_J^{*N}, r_s\right)$

b) Input: r_s; $\Sigma_J^{*N} = \left(t_J, \vec{R}_J^{*N}, \vec{V}_J^{*N}\right)$

c) Output: $\Sigma_J^{*X} = \left(t_J, \vec{R}_J^{*X}, \vec{V}_J^{*X}\right)$

d) Computations:

$$\sigma_J^{*N} = G^{-1}\left(\Sigma_J^{*N}\right)$$

$$\sigma_N^c = L_N\left(\sigma_J^{*N}, r_s\right)$$

$$\sigma_X^c = C_X\left(\mu_m, \sigma_N^c, r_s\right)$$

$$\sigma_J^{*X} = L_t\left(\sigma_X^c, t_J\right)$$

$$\Sigma_J^{*X} = G\left(\sigma_J^{*X}\right)$$

e) Comments:

When propagating a real prepericynthion state vector to a point on the postpericynthion leg of the real trajectory, the pseudostate must be transferred from the geocentric prepericynthion conic to the postpericynthion conic at or near the real pericynthion passage time (within ± one hour, for typical lunar mission trajectories).

E-2 POSTPERICYNTHION-TO-PREPERICYNTHION

a) Notation: $\Sigma_J^{*N} = N_X\left(\Sigma_J^{*X}, r_s\right)$

b) Input: r_s; $\Sigma_J^{*X} = \left(t_J, \vec{R}_J^{*X}, \vec{V}_J^{*X}\right)$

c) Output: $\Sigma_J^{*N} = \left(t_J, \vec{R}_J^{*N}, \vec{V}_J^{*N}\right)$

d) Computations:

$$\sigma_J^{*X} = G^{-1}\left(\Sigma_J^{*X}\right)$$

$$\sigma_X^c = L_X\left(\sigma_J^{*X}, r_s\right)$$

$$\sigma_N^c = C_N\left(\quad, \sigma_X^c, r_s\right)$$

$$\sigma_J^{*N} = L_t\left(\sigma_N^c, t_J\right)$$

$$\Sigma_J^{*N} = G\left(\sigma_J^{*N}\right)$$

e) Comments:

When propagating a real postpericynthion state vector to a point on the prepericynthion leg of the real trajectory, the pseudostate must be transferred from the geocentric postpericynthion conic to the prepericynthion conic at or near the real pericynthion passage time (within ± one hour, for typical lunar mission trajectories).

REFERENCES

1. S. W. Wilson, Jr., "Overlapped Conic Simulation of Three-Body Trajectories," TRW IOC 5524.10-3, 31 March 1969.

2. P. A. Penzo, "Translunar First Guess Logic Utilizing the Overlapped Conic Technique," TRW IOC 5520.9-16, 25 June 1969.

3. P. A. Penzo, "Use of the Impact Parameter and the Overlapped Conic to Targeting Translunar Trajectories From a Midcourse State," TRW IOC 5520.9-11, 22 April 1969.

4. T. E. Suttles, "Calibration of Analytic Lunar Programs," TRW 3832-6002-RU000, 15 August 1965.

5. P. R. Escobal, et al, "The Hybrid Patched Conic Technique Applied to Translunar and Transearth Trajectory Propagation," TRW 69-FMT-728 (11176-6037-R0-00), 10 February 1969.